JOURNAL OF GEOPHYSICAL RESEARCH, VOL. 112, D12111, doi:10.1029/2006JD008135, 2007

Simultaneous observation of noctilucent clouds, mesospheric summer echoes, and temperature at a midlatitude station (54°N)

M. Gerding,[1] J. Höffner,[1] M. Rauthe,[1] W. Singer,[1] M. Zecha,[1] and F.-J. Lübken[1]

Received 10 October 2006; revised 7 March 2007; accepted 3 April 2007; published 23 June 2007.

[1] Between 2003 and 2005, 12.9 h (8 events) of noctilucent clouds (NLC) and 250 h of mesospheric summer echoes (MSE) were observed above Kühlungsborn (54°N, 12°E) by lidar and radar, respectively. The ice-layer seasons typically last for 50 (NLC) and 70 days (MSE). The observations are compared with simultaneous lidar temperature soundings. Altogether, 79 soundings were performed in the periods 10 May to 8 August of each year. These profiles revealed a minimum mesopause temperature of 145 K at 87 km shortly after summer solstice. The mean temperatures are below the frost point temperature for a period of ~15 days after summer solstice and in the altitude range ~85–89 km. Simultaneous observations of temperature, MSE/NLC, and winds by radar and lidar show that ice particles occur primarily during southward winds and during the cold phases of gravity waves and tides, providing temperatures up to ~20 K lower than the mean. Water vapor saturation profiles are calculated from the temperatures and modeled water vapor concentrations, showing that the ice layers occur at the bottom of the supersaturated region. Only about one fifth of all supersaturation events below 85 km in fact yield NLC above our site. Even saturation ratios of 10–100 lasting for at least 4 h do not necessarily lead to the formation of NLC. We conclude that NLC at midlatitudes are strongly coupled to the advection of preexisting ice particles from northern latitudes. If the ice particles have sublimated prior to the observation, they do not form again even in the cold phases of waves.

Citation: Gerding, M., J. Höffner, M. Rauthe, W. Singer, M. Zecha, and F.-J. Lübken (2007), Simultaneous observation of noctilucent clouds, mesospheric summer echoes, and temperature at a midlatitude station (54°N), *J. Geophys. Res.*, *112*, D12111, doi:10.1029/2006JD008135.

1. Introduction

[2] About 120 years ago, first observations of noctilucent clouds (NLC) near the midlatitude northern horizon were initially published by *Leslie* [1885] and later also by *Jesse* [1885] and *Backhouse* [1885]. In the following decades, numerous sightings took place, mostly limited to midlatitudes because of the requirement of twilight or predawn conditions for naked-eye observations. In the last decades, extensive lidar, radar, satellite, and rocket experiments have shown that noctilucent clouds (or more general polar mesospheric clouds, PMC) are mainly a phenomenon at polar latitudes. Here ice crystals are formed in the mesopause region at temperatures below ~150 K. By multi-instrument soundings, the understanding of NLC formation has been strongly improved, as for example, described in the review by *Thomas* [1991]. It is established that ice particles can also form so-called (polar) mesospheric summer echoes, (P)MSE when they are charged and spatially structured (see, e.g., review by *Rapp and Lübken* [2004]).

[3] *Taylor et al.* [2002] and *Thomas* [2003] indicated that northern hemispheric NLC in recent years may have extended further south compared to previous years. On the other hand, for example, *Avaste et al.* [1980] had described repeated observations of NLC down to 45°N already in the 1970s. A possible connection between (P)MSE occurrence and equatorward winds has been indicated by *Singer et al.* [2003] and only recently examined by *Morris et al.* [2007]. Because possible changes in NLC may be related to trends in temperature, water vapor concentration, or meridional winds (and by this to "global change"), the mechanisms for NLC existence in midlatitudes need to be understood in detail. Obviously, NLC and MSE at midlatitudes are a rare phenomenon compared to polar latitudes [*Thomas et al.*, 1994; *Latteck et al.*, 1999; *Alpers et al.*, 2000; *Wickwar et al.*, 2002; *Zecha et al.*, 2003; *Lübken et al.*, 2004]. Midlatitude summer temperatures in the mesopause region are higher, and the saturation of water vapor is smaller. For Kühlungsborn (54°N, 12°E), *She and von Zahn* [1998] and *Latteck et al.* [1999] report temperatures higher than the frost point temperature at 86 and 85 km altitude, respectively. Model studies show that temperatures below the frost point can occur within gravity and tidal waves [*Rapp et al.*, 2002; *Berger and Lübken*, 2006], allowing the existence of pre-formed ice particles. Unfortunately, many temperature measurements in the summer mesopause region (for example, by satellite instruments) have a vertical resolution of ~2–4 km, i.e., larger than the typical vertical

[1] Leibniz-Institute of Atmospheric Physics, Kühlungsborn, Germany.

0148-0227/07/2006JD008135$09.00

Table 1. Overview on the Lidar Systems at IAP Kühlungsborn for NLC and Temperature Soundings

	RMR Lidar	K Lidar	Na Lidar
Laser Type	Nd:YAG	Alexandrite	Dye (2×)
Wavelength, nm	1064/532/355	770	589
Pulse Energy, mJ	500/400/200	120	2 × 25
Repetition Rate, Hz	30	35	30
Integration Time for NLC, min	2.5	2.5	2.5
Altitude Resolution for NLC, km	0.2	0.2	0.2
Integration Time for *T*, min	>15	>15	–
Altitude Resolution for *T*, km	0.2–1	0.2–1	–

scale of NLC (full width at half maximum or FWHM = 1.2 km, *Fiedler et al.* [2003]). To the best of our knowledge, at midlatitudes (here defined as 40°–60°N/S), simultaneous temperature and NLC soundings do not exist.

[4] In this paper, we present lidar temperature measurements in the upper mesosphere and lower thermosphere in summer at Kühlungsborn (54°N, 12°E). Besides the mean temperature of the summer mesopause region, we describe temperature soundings in the vicinity of NLC and MSE with high spatial and temporal resolution. Using water vapor results from a circulation model, we calculate the degree of water vapor saturation. We will interpret the saturation profiles in combination with meteor radar wind data and discuss implications for ice existence and formation above our station.

2. Observational Techniques and Analyses

[5] At Kühlungsborn, a Rayleigh-Mie-Raman (RMR) lidar and a potassium (K) resonance lidar are operated to measure temperatures from 1 to 105 km altitude and optical parameters of NLC [*von Zahn and Höffner*, 1996; *Alpers et al.*, 2000, 2004; *Rauthe et al.*, 2006]. These lidars are complemented by a dye laser system solely for NLC soundings at a sodium resonance line [e.g., *Gerding et al.*, 2000]. The lidars are co-located with a radar for MSE detection and meteor wind soundings [*Latteck et al.*, 1999; *Singer et al.*, 2003; *Zecha et al.*, 2003]. Lidar-observed temperature data are combined with model estimates of water vapor concentrations [*Sonnemann and Grygalashvyly*, 2005] with background conditions from the Leibniz-Institute Middle Atmosphere model LIMA (U. Berger, Modeling of middle atmosphere dynamics with LIMA, submitted to *Journal of Atmospheric and Solar-Terrestrial Physics*, 2007, hereinafter referred to as Berger, submitted manuscript, 2007). We apply the vapor pressure formula of *Marti and Mauersberger* [1993] and air density from the MSISE-90 atmosphere [*Hedin*, 1991].

2.1. Description of Lidars and Temperature Retrieval

[6] The RMR lidar is composed of a Nd:YAG laser emitting laser radiation at 1064, 532, and 355 nm wavelength. Typically, NLC soundings are performed at visible and UV wavelengths only because at our site, NLC backscatter at 1064 nm is too weak to be separated from the background [cp. *Alpers et al.*, 2000]. All soundings of the RMR lidar described here are limited to nighttime (darkness) conditions because the signal-to-noise-ratio during daytime is not sufficient for mesospheric soundings. The K lidar has been designed to measure temperatures in the altitude of the potassium layer (~85–105 km) during day and night [*von Zahn and Höffner*, 1996; *Fricke-Begemann et al.*, 2002]. NLC are detected as a by-product, providing an additional wavelength (770 nm) for the calculation of aerosol properties. The soundings are complemented by a sodium lidar system, probing the NLC at an additional wavelength (589 nm). This lidar consists of two dye lasers simultaneously pumped by one excimer laser [cp. *Gerding et al.*, 2000]. Typical pulse energies, repetition rates, and integration times for all lidars are given in Table 1.

[7] The simultaneous observations of the K lidar and the RMR lidar are combined to retrieve continuous temperature profiles from 1 to ~105 km altitude [*Alpers et al.*, 2004; *Rauthe et al.*, 2006; *Gerding et al.*, 2007]. In the following, we will concentrate on the NLC region and the adjacent ranges of the upper mesosphere and lower thermosphere. At ~85–105 km, temperatures are derived from the spectral broadening of the 770-nm K-D_1 resonance line [*von Zahn and Höffner*, 1996]. The RMR lidar measures a relative density profile from the backscatter signal at 532 nm. This density profile is converted into a temperature profile assuming hydrostatic equilibrium. The start temperature for the retrieval at the upper end of the integration range (~89 km) is taken from the simultaneous, colocated K lidar observations. A typical integration time for temperature soundings is 30–60 min for both lidars. The altitude resolution is 0.2–1 km. An altitude- and signal-dependent smoothing filter of 0.4 to 3 km width is applied. Figure 1

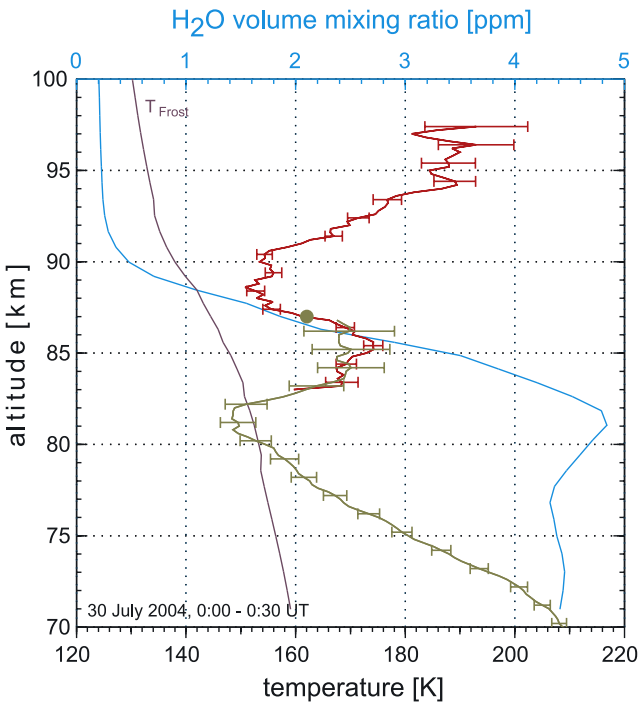

Figure 1. Temperature profile measured by the potassium lidar (red) and RMR lidar (green) at 30 July 2004 (integration time, 30 min; altitude resolution, 200 m). At around 85 km, both methods overlap. The start temperature for the Rayleigh integration method is given by the K lidar at 87 km altitude as indicated by the green dot. Horizontal line, statistical error; only every fifth error bar is plotted. For comparison, the water vapor mixing ratio (blue, upper scale) and the frost point temperature (purple) are shown from the LIMA model for 30 July.

gives an example of a combined temperature profile in the altitude range between 70 and 100 km from 30 July 2004, using 30-min and 0.2-km resolution. Taking the statistical error of the RMR lidar between 83 and 87 km into account, the temperature measurements of the K lidar and RMR lidar agree nicely. The statistical error is less than 5 K for the whole range below 95 km even with this high spatial and temporal resolution. Although the temperature is slightly below the frost point temperature in a small altitude range between 80–82 km, no NLC was observed in this example.

2.2. Temperature Retrieval in the Vicinity of NLC

[8] The combination of K lidar and RMR lidar yields temperature data in the whole upper mesosphere and lower thermosphere with a vertical resolution of 1 km. Unfortunately, the standard retrieval is limited to NLC-free conditions for the following reasons:

[9] 1. The Doppler resonance method is limited to the K layer range. *Plane et al.* [2004] and *Lübken and Höffner* [2004] have shown that ice particles significantly reduce the number of metal atoms in a particular range. Therefore the K lidar is only able to measure temperatures in the absence of 'large' ice particles like NLC.

[10] 2. The RMR lidar measures a relative density profile (and by this temperature) only in the range of pure molecular scattering. NLC provide additional aerosol scattering. In the presence of aerosols, the backscatter profile can not a priori be used as a measure for the molecular density. An aerosol correction by the inelastic N_2 Raman backscatter can not be applied in the upper mesosphere because of the small Raman signal level. Therefore temperatures can not be retrieved directly within the NLC. The Rayleigh signal has to be interpolated within the NLC layer to allow for hydrostatic temperature calculation below. A summary of the method is presented below; for details, see the study of *Gerding et al.* [2007].

[11] Above the NLC layer, temperatures are calculated from the K resonance and Rayleigh signal as described for non-NLC conditions. Within NLC with $\beta(532) > 0.1 \cdot 10^{-10}$ $m^{-1}sr^{-1}$, the Rayleigh signal is interpolated by a polynomial. After this procedure, the standard temperature retrieval is performed. Temperature data are used only below the interpolated range, while within NLC altitudes, effects of the applied polynomial remain [*Gerding et al.*, 2007]. We use this procedure only for NLC layers with up to 2.5 km thickness. For more extended NLC, an effect of the interpolation procedure remains visible even some kilometers below the NLC. NLC with $\beta(532) < 0.1 \cdot 10^{-10}$ $m^{-1}sr^{-1}$ can typically not be resolved by our lidars. The effects of such weak NLC on the Rayleigh temperature retrieval are on the same order as the statistical error in this altitude range and are therefore neglected here.

2.3. Radar and Wind Retrieval

[12] Electron density fluctuations in the mesosphere can result in irregularities of the refraction index of half the radar wavelength and thereby create backscattering of radar waves in the very-high-frequency (VHF) band, known as (polar) mesosphere summer echoes, (P)MSE [*Ecklund and Balsley*, 1981]. The ice particles in the summer mesopause region prevent the fast destruction of these small irregularities by a reduction in the electron diffusivity. These echoes were observed with the OSWIN MST (Mesosphere/Stratosphere/Troposphere) radar operated at 53.5 MHz at Kühlungsborn since 1998. The radar system was designed for unattended continuous operation starting with a peak power of 36 kW in 1998 and continuing with a peak power of 72 kW in 2000. The phased antenna array consists of 144 four-element Yagi antennas with a one-way half-power beam width of 6°. Generally, radar observations are performed using tilted and vertically directed radar beams with over-all sequence duration of 2–4 minutes. Mesospheric studies were done in an altitude range of about 70 to 100 km with a range resolution of 300 m. A 16-bit complementary code has been applied to utilize the available duty cycle of 5%. MSE observations have been done during the summers of 1998 and 2000 to 2005 [*Latteck et al.*, 1999; *Zecha et al.*, 2003]. These measurements were completed by additional meteor wind observations since April 2004 [*Singer et al.*, 2003]. An interleaved operation between MST mode and meteor mode was applied.

[13] In meteor mode, a different antenna system is used for transmission and reception. The all-sky meteor-detection antenna system utilizes crossed antenna elements to ensure a near azimuthal sensitivity to meteor echoes. A three-element Yagi antenna is used on transmission. On reception, a five-antenna interferometer provides a range resolution of 2 km and an angular resolution of 2° in meteor location. From each meteor, the radial velocity of the meteor trail due to its movement with the background wind is estimated. Data bins of 1 h in time and 3 km in altitude are used to determine horizontal winds between 80 and 96 km. An all-sky least squares algorithm is used in each bin to estimate the mean zonal and meridional wind from the measured radial velocities (for details, see *Hocking and Thayaparan* [1997]).

[14] Comparisons of NLC and MSE observations are limited because MSE are typically restricted to daytime because of the higher number of free electrons produced by solar irradiance. At Kühlungsborn, only the K lidar has daytime (temperature) capabilities, but most NLC at this site are too weak to be observed by the lidar at 770 nm. In the following, we will concentrate on comparisons (1) between MSE and K lidar temperatures and (2) between NLC and continuous (K and RMR lidar) temperature profiles below/above the aerosol layer. During both day and night, the observations are complemented by wind data from meteor soundings by the OSWIN radar.

3. Mean Summer Temperatures above Kühlungsborn

[15] Temperature measurements by lidar were performed in a total of 240 nights within the years 2003–2005. The mean temperatures in the upper mesosphere and mesopause region are shown in Figure 2 for the period between 10 April and 17 September (days 100 and 260, respectively). The nightly mean profiles are smoothed by a running mean of ±20 days and ±3 km. From the data set, we derived a summer period that is based on the temperature at 85 km altitude. This altitude is of particular importance as it is the mean altitude of MSE above Kühlungsborn [*Zecha et al.*, 2003]. We define "summer" as the period where $T_a - T_w \leq T_f$, with T_a the average temperature at 85 km, T_w the typical tidal and gravity wave amplitude (i.e., ~10 K, see below),

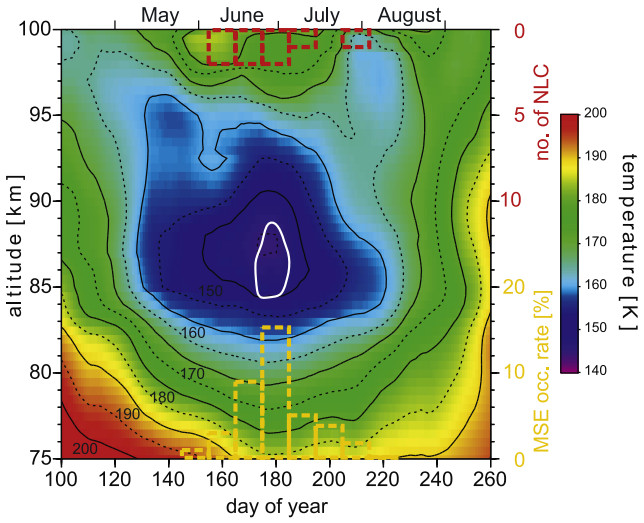

Figure 2. Mean temperatures between 75 and 100 km above Kühlungsborn from lidar soundings between 2003 and 2005. Thick black isolines are at 10 K interval. For ~2 weeks in midsummer, temperatures are below the frost point (white isoline). A running mean of ±20 days is applied on the night mean profiles. The yellow and red histograms mark the typical periods of MSE and NLC occurrence, respectively (occurrence rates given on the right axis).

and T_f the frost point temperature (~150 K). Therefore the summer is characterized by $T_a \leq 160$ K and extends from day 130 to day 220 (10 May to 8 August), clearly distinguishable from the "spring" and "autumn" with their higher temperatures. The summer period also coincides with the period where the mesopause is in the lower, summer state around 87 km. In Figure 2, temperatures below the frost point (i.e., $S \geq 1$) are marked by a white isoline, assuming altitude-dependent water vapor concentrations of ~0.5–4.5 ppmv (between 90 and 80 km, respectively). The lowest temperatures of all are observed at the end of June with ~145 K at 87 km altitude. At NLC altitudes (83 km), mean temperatures are mostly higher than ~155 K. Obviously, from the average state of the mesopause region (and neglecting waves) ice particles should only exist for ~15 days shortly after summer solstice in the altitude range 85–89 km. This is well above typical NLC altitudes. The average temperatures during the NLC and MSE periods are observed as high as 163 and 165 K in 83 and 85 km altitude, respectively, i.e., up to ~15 K higher than the frost point temperature. In summary, average temperatures are too large for the existence of ice particles at 83–85 km, i.e., at typical NLC and MSE altitudes. To examine this apparent contradiction, we will describe time-dependent temperature soundings in the vicinity of MSE and NLC in the next section.

4. Case Studies of Simultaneous Observations of Temperatures, NLC, and MSE

4.1. Observations of MSE and Daylight Temperatures at 15 July 2003

[16] Mesospheric summer echoes (MSE) were observed on several occasions since 1998 by the OSWIN radar. In Figure 3a, MSE of nearly 5 h duration on 15 July 2003 is presented. The altitude of the echo decreases by up to 4 km in less than 2 h, what we take as an indication of a downward-progressing phase of a wave. The average thickness remains constant at ~3 km. The MSE disappears around 14 UT at 82 km altitude and does not appear again for the next 26 h (not shown here).

[17] The potassium lidar was switched on around 11:30 UT after tropospheric clouds disappeared and measured until ~17:30 UT. The K layer extended down to 82–84 km. As can be seen in Figure 3, temperatures change very fast, for example, by more than 30 K within 2 h in ~88 km. For the whole time of simultaneous MSE and temperature soundings, the MSE is below a warm layer, changing height with the same phase speed as the wave (Figure 3). The altitude of the MSE is in rough agreement with the region of supersaturation. Comparatively high temperatures of ~160 K are measured until 12:30 UT in the upper part of the MSE. However, here the radar echo is very weak, and the ice particles may already sublimate in the downward-propagating phase of the wave. Note that even outside of the MSE range, temperatures are very low (~125–122 K), in particular around 88 km (13:30–14:30 UT) and 85 km (15:00–16:00 UT). However, although supersaturation of more than a factor of 100 is present in both cases for at least ~1 h, no MSE or NLC develops at those altitudes possibly because time is too short for the formation of fresh ice particles.

4.2. Simultaneous Observation of Temperatures and NLC at 30 July 2004

[18] On 30 July 2004, an NLC appeared between 01:27 and 02:20 UT at an altitude of ~80 km. It was the latest-ever NLC event above our station, and the backscatter coefficient was moderately strong (mean value β_{532} =

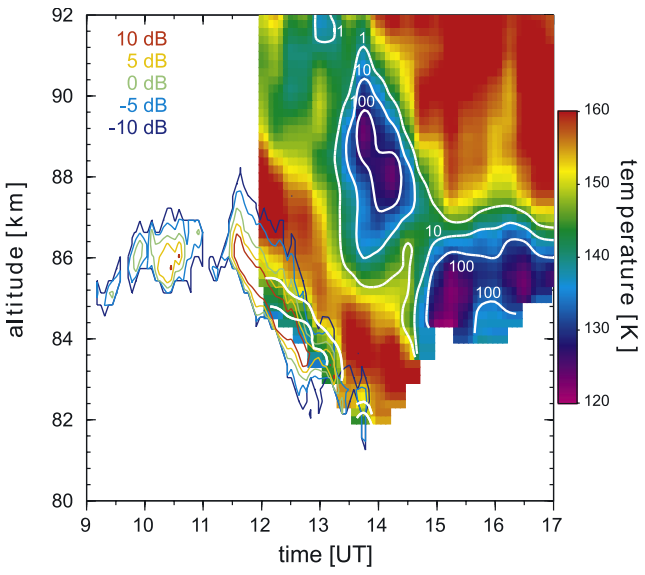

Figure 3. Simultaneous observation of MSE (colored isolines) and temperature (color coded) during 15 July 2003 by the OSWIN radar and K lidar, respectively. The saturation ratio is plotted by white isolines (S = 1, 10, and 100).

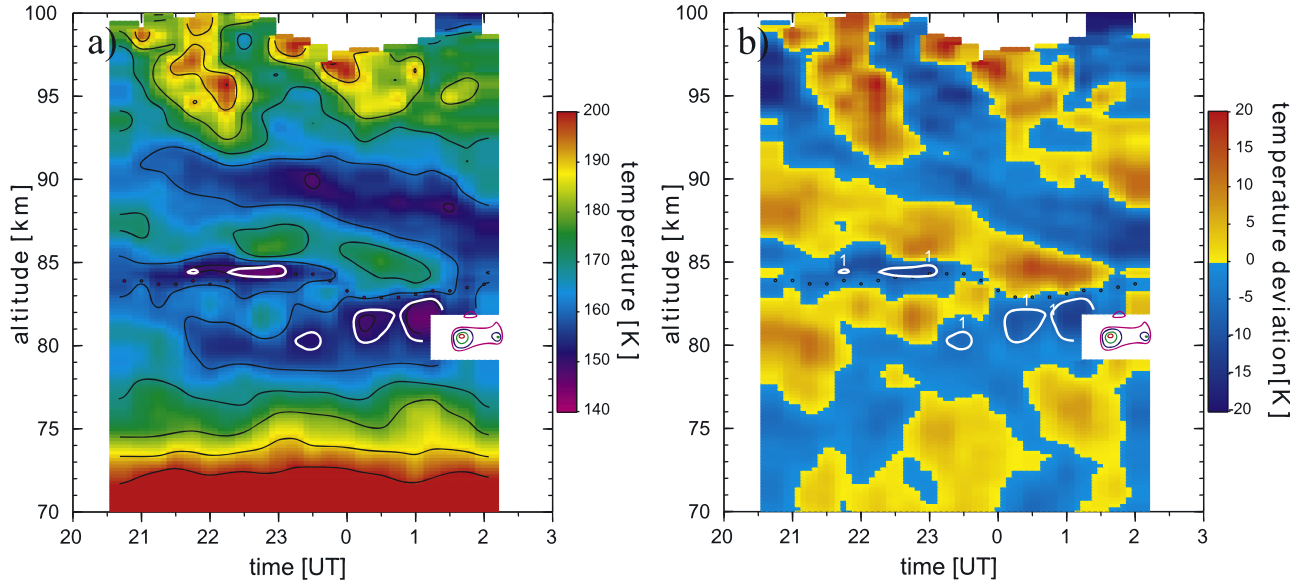

Figure 4. Simultaneous observation of NLC (colored isolines) and temperature (color coded, black isolines at 10 K contour interval) during 29/30 July 2004; (a) absolute temperature and (b) temperature deviation from the night mean profile. The black dots mark the transition of the temperature retrievals. White isolines mark the regions with saturation ratio $S = 1$. The NLC is represented by the backscatter coefficient at 532 nm (β_{532}). The colored isolines are at $\beta_{532} = 0.2/1.0/3.0/5.0 \cdot 10^{-10}$ $m^{-1}sr^{-1}$.

$3.1 \cdot 10^{-10}$ $m^{-1}sr^{-1}$). As can be seen from Figure 4, the temperature field is highly structured throughout the whole night, with thick cold layers around 80 and 90 km (∼150 K and less) and a temporary thin layer around 85 km. In between these cold regions, temperature rises by ∼20 K. Supersaturation is observed in a 1-km range around 84.5 km and between ∼80–83 km. Eventually, the NLC appears at 80.5 km at the lower edge of the weakly supersaturated region.

[19] In Figure 4b, the deviation of the temperature from the nightly mean is plotted. Wave disturbances with amplitudes of up to ±15 K can easily be identified, for example, gravity waves with periods of ∼1 h (best visible around 82 km) and ∼4 h (around 88 km). Especially the longer periods are typical for our location [*Rauthe et al.*, 2006]. Usually, downward phase progression is seen in our lidar data. However, during the night of 29/30 July 2004 (Figure 4), an upward propagating cold phase is visible below 83 km. Temperatures fall below the frost point after 23 UT when this cold phase reaches potential NLC altitudes. The short period wave mentioned above modulates the temperature field (and by this, S) in 80–83 km as well as the NLC brightness.

4.3. Simultaneous Observation of Temperatures and NLC at 22/23 June 2005

[20] We now present another case of NLC observation which underscores that NLC typically occur at the lower edge of the supersaturated region. On 22/23 June 2005, a NLC was detected during the whole time of RMR lidar operation (22:40–01:30 UT, see Figure 5). Measurements by the potassium and RMR lidars reveal temperatures below the frost point in a broad range between 84–90 km throughout the whole night. Saturation ratios up to $S \approx 16$ are observed above the NLC. Below the NLC, more precisely at 81 km, temperatures are 154–162 K, i.e., always above the frost point temperature. It will be shown later that from our observations the degree of saturation is typically larger than one above the NLC and lower below, as it is also known from other stations [e.g., *Lübken et al.*, 1996 and references therein].

[21] At the end of the sounding (∼02:25 UT), the temperature above the NLC is still below the frost point by ∼13 K in 87 km altitude. Though the RMR lidar terminated operation at 01:30 UT because of morning twilight, the potassium lidar was in operation for another 55 min and detected the NLC until it stopped sounding. It should be noted that this NLC observation was the second longest measured at Kühlungsborn (3:45 h).

[22] Temperatures below the NLC region reveal again downward propagating wave energy (upward propagating phase), while the other NLC in the summers 2004 and 2005 were observed during (normal) upward wave progression (not shown here). The dominating wave period during the night of 22/23 June 2005 is longer than the RMR lidar observation time (∼3 h) and can therefore not be determined exactly.

4.4. Summary of Simultaneous NLC and Temperature Observations

[23] The case studies described above clearly show that the NLC above our midlatitude location are observed at the lower edge of the supersaturated range. The same is true for practically all NLC where temperatures are available. Table 2 gives an overview on six cases during the years 2004 and 2005. One additional sounding with NLC (12/13 June 2003) was too short to allow temperature calculation, whereas the NLC on 29/30 June 2005 was vertically thicker than 2.5 km and does not allow the interpolation of the Rayleigh signal and by this a temperature calculation. During

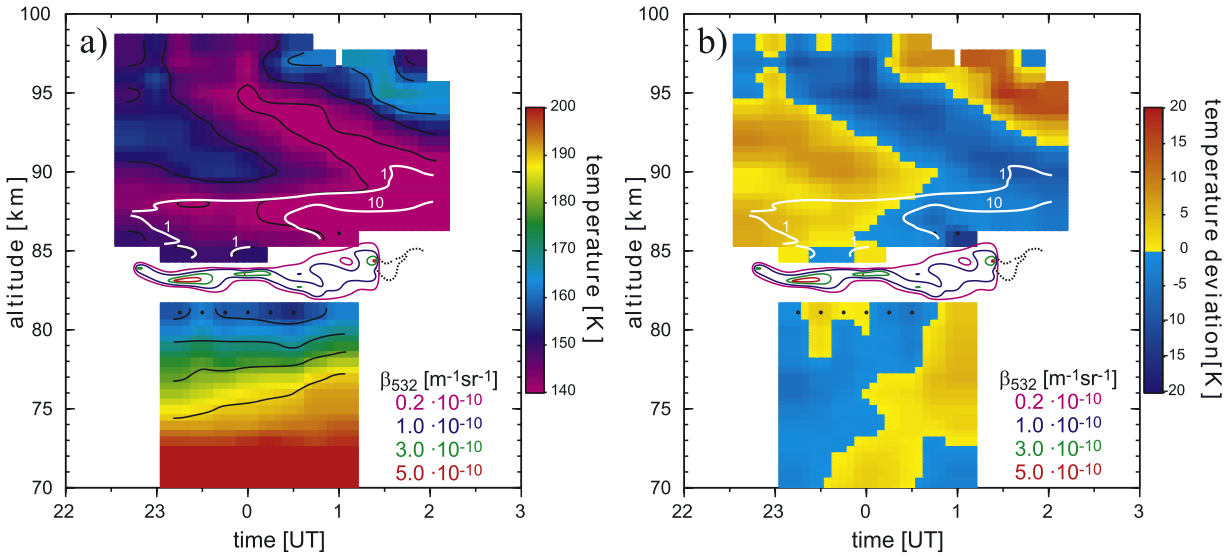

Figure 5. Simultaneous observation of NLC (colored isolines) and temperature (color coded, black isolines at 10 K contour interval) during 22/23 June 2005; (a) absolute temperature and (b) temperature deviation from the night mean profile. The black dots mark the transition of the temperature retrievals. White isolines mark the regions of constant saturation ratio. The NLC is represented by the backscatter coefficient at 532 nm (β_{532}) as given in the legend. After the shutdown of the RMR lidar at 1:30 UT, the NLC data of the K lidar data are plotted (dotted black isoline: $\beta_{770} = 0.3 \cdot 10^{-10}$ m^{-1}sr^{-1}).

two NLC events in 2005, the temperature changed strongly during the observation. Therefore we have calculated different saturation ratios for the beginning and the end of the events. Except for the NLC on 7/8 June 2005, the temperature above the NLC is always below the frost point ($S \geq 1$). On 7 June 2005, a saturation ratio of $S \approx 50$ was observed prior to the appearance of NLC in our lidar. It remains speculative whether the air was still supersaturated just within the NLC range or whether the NLC was actually sublimating during the advection to our site.

[24] In six out of the eight periods, the air was undersaturated below the NLC. In the remaining NLC night (9/10 July 2005, both examined periods), the saturation ratio was at least smaller below than above the NLC. During all events, the maximum of supersaturation was 1–5 km above the NLC. We therefore conclude from our data set that the NLC above our site are generally observed at the lower edge of a supersaturated region. As mentioned above, this has already been shown for polar latitudes [see e.g., *Lübken et al.*, 1996 and references therein], but such evidence for midlatitude NLC was up to now unavailable.

Table 2. Saturation Ratios Above and Below the NLC for all Events With Simultaneous Temperature Measurements[a]

Date	Time	z_a, km	$S(z_a)$	z_b, km	$S(z_b)$	$z(S_{max})$, km	S_{max}
12/13 June 2003	n.a.	n.a.	n.a.	n.a.	n.a.	n.a.	n.a.
01/02 July 2004	00:45-01:45	86	47	81	0.2	87	205
29/30 July 2004	01:45-02:15	82	2.4	78	<0.1	82	2.4
07/08 June 2005	00:00-01:00	85	0.3	82	<0.1	85	0.3
13/14 June 2005	00:15-01:15	86	9.2	81	0.1	87	41
22/23 June 2005	23:00-00:00	85	1.0	81	0.1	88	3.0
	00:00-01:00	86	4.2	81	0.7	87	16
29/30 June 2005	n.a.	n.a.	n.a.	n.a.	n.a.	n.a.	n.a.
09/10 July 2005	23:30-00:30	84	2.4	80	1.2	85	5.1
	00:30-01:30	84	1.5	80	1.0	85	2.0

[a] z_a, lowest bin above NLC; z_b, highest bin below NLC; $z(S_{max})$, altitude bin of highest saturation ratio; n.a., no temperature data available.

4.5. Temperature Observations at 24/25 June 2005

[25] In the previous sections, some examples have been presented showing the supersaturation in some temporal and spatial connection with NLC. In fact, these events are in good agreement with the general assumptions on NLC formation and existence. However, there were also various observations in the summers of 2003–2005, where temperatures were observed below the frost point but where no NLC was detected by the lidar (see Figure 6). In fact, in the majority of soundings with sufficiently low temperatures, the lidars do not observe any NLC.

[26] In the night of 24/25 June 2005, an impressive NLC display was visible at Kühlungsborn and also in large parts of mid-Europe. Even observers several hundred kilometers southwest of our location reported visual NLC sightings (listed for example, on the Web page of Tom McEwan, http://www.nlcnet.co.uk/index.htm). The unusual extension of the NLC might be connected with two rockets malfunctioning after launch in northeast Europe on 21 June 2005 (cf. for example, "Jonathan's Space Report" at http://www.planet4589.org/space/jsr/jsr.html) and injecting possibly additional water vapor into the middle atmosphere. The K lidar and the RMR lidar at Kühlungsborn were in operation between 20:45 and 01:45 UT and between 21:13 and 01:30 UT, respectively. Figure 6 shows the observed temperature profiles and the calculated saturation ratios. Very low temperatures of ~132 K are observed at 87 km altitude (0:30 UT), and the air is highly supersaturated at 85 km during the whole 5-h sounding period. Partly, the supersaturated region extends from 81 to 89 km. Most of the time, the saturation ratio in the center of the cold region exceeds $S = 10$, and partly it is even larger than $S = 100$.

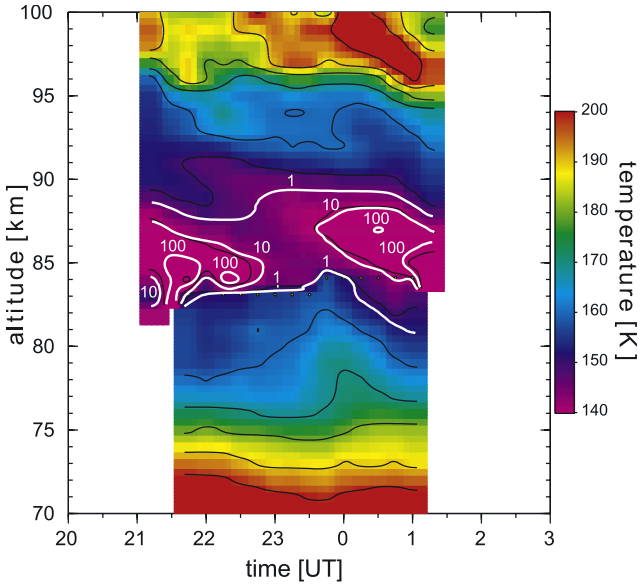

Figure 6. Temperature observation during the night of 24/25 June 2005. White isolines mark the regions of constant saturation ratio.

Remarkably, despite this high supersaturation, we have not observed any NLC. The OSWIN radar detected MSE in the afternoon of 24 June and in the morning of 25 June but not in the sunlit hours just before and after the lidar observation of the low temperatures (see below). Therefore there is no indication that an ice layer below the detection limit of our lidars existed during the lidars' operation time.

4.6. Wind Observations During Nights With and Without NLC

[27] During the described cases in 2005 with and without NLC, the OSWIN radar performed wind measurements. These observations are used to examine the role of horizontal advection for the existence of ice particles and supersaturated periods. The OSWIN soundings during the NLC on 22/23 June 2005 yield a southward meridional wind of 10–20 m/s and a westward zonal wind of up to 50 m/s. Figure 7 shows the meridional wind during a 48-h period, i.e., before, during, and after the NLC. The NLC is observed after several hours of southward directed wind; that is, the observed air parcel is advected from polar latitudes (~400 km within 6 h). Also, the MSE is observed only during southward wind periods, while it vanishes during northward-directed meridional wind.

[28] On 24 June 2005, again, the meridional wind component was most often negative (southward) below 88 km (Figure 8). The southward wind was largest during the period of supersaturation around midnight UT (>40 m/s absolute). In the morning hours of 25 July 2005, the wind turned, and the meridional component changed to northward. The MSE was observed during a calm northward component (~20 m/s). During 25 June, a periodical change in the meridional wind component due to tidal waves was observed in the whole altitude range. Overall, the meridional wind field below 85 km is comparable to the situation of two nights before, where NLC were observed by lidar (cp. Figure 5). Therefore in the examined cases, a

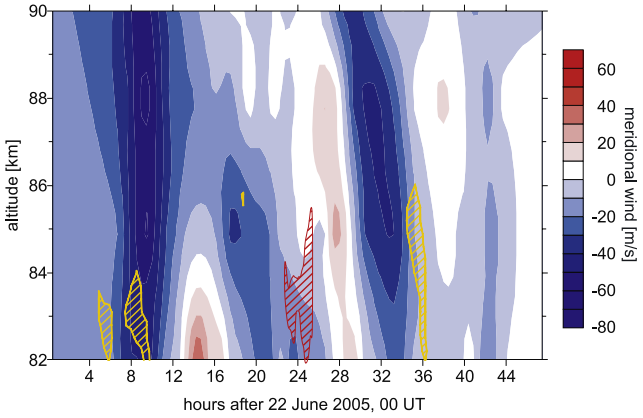

Figure 7. Meridional winds on 22/23 June 2005 as observed by the OSWIN meteor radar (color coded). The resolution is 3 km and 60 min in space and time, respectively. The hatched areas show the MSE (OSWIN, yellow) and NLC (lidar at 532 nm, red).

southward wind component seems to be necessary for the existence of ice particles, while it is not sufficient. Even if the temperatures are low enough above our site and the air is advected from the north, we might still not observe any NLC or MSE. We will present a statistical study based on the whole data set below.

5. NLC Statistics and Comparison With Winds and Wave Amplitudes

5.1. Statistics on NLC

[29] Between 2003–2005, eight nights with noctilucent clouds were detected by our lidars at Kühlungsborn. This number is comparable to previous seasons, where the sensitivity of the systems was slightly lower. Between 1997 and 2001, a total of seven NLC were observed by lidar. The strongest events are described by *Alpers et al.* [2000, 2001]. In 2000 and 2002, no NLC were observed. The lower signal strength of the RMR lidar before 2003 inhibits the retrieval of temperature profiles above and

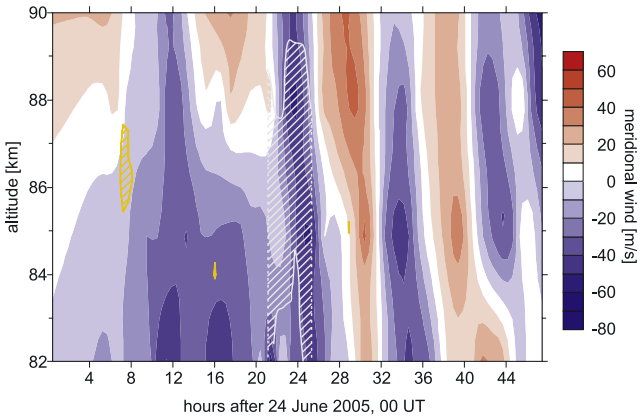

Figure 8. Meridional winds on 24/25 June 2005 as observed by the OSWIN meteor radar (color coded, cp. Figure 7). The hatched areas show the MSE (OSWIN, yellow) and supersaturated region (gray).

Table 3. NLC Observations During the Summers of 2003–2005 at Nighttime by the Kühlungsborn Lidars[a]

Date	Altitude, km	R_{max}	β_{max} 10^{-10} $m^{-1}sr^{-1}$
12/13 June 2003	80.8	2.6	0.4
01/02 July 2004	84.2	4.4	0.6
29/30 July 2004	80.5	13.3	3.3
07/08 June 2005	83.8	3.0	0.4
13/14 June 2005	83.7	17.7	3.2
22/23 June 2005	83.4	11.5	2.0
29/30 June 2005	85.1	2.9	0.3
09/10 July 2005	82.2	3.4	0.5

[a]Centroid altitude, maximum backscatter ratio (R_{max}), and maximum backscatter coefficient (β_{max}) at 532 nm are given as averaged for the particular event.

below the NLC. Only the data from the K lidar is available for the altitude range above the NLC. From the retrieval of optical parameters of the NLC, we get evidence that the NLC events before and after 2003 are generally comparable in terms of altitude, NLC thickness, and brightness (backscatter coefficient). Table 3 summarizes the mean NLC parameters since 2003 (altitude, backscatter ratio, and backscatter coefficient) as derived from the 532-nm backscatter. For four soundings, the NLC signal was strong enough to allow detection with at least three wavelengths (770 nm, 532 nm, 355 nm, and/or 589 nm). Particle mode radii of ~40 nm and number densities of ~350 cm^{-3} are derived, assuming spherical particles and a Gaussian size distribution. These assumptions are of course questionable. Unfortunately, even for the stronger NLC, the signal is too low to distinguish between Gaussian and lognormal size distributions as well as different particle shapes. Therefore we do not want to contribute to the discussion on particle shapes but state that for the stronger NLC, the parameters observed above Kühlungsborn are in the range of observations at other stations.

[30] Three additional observations of NLC during daytime by the potassium lidar are not examined here because the K lidar provided temperatures only above the NLC. Missing data directly above and below the NLC inhibit an evaluation of supersaturation in the vicinity of the NLC.

[31] Table 3 reveals a more or less even distribution of NLC throughout the summer season. Figure 2 shows a histogram of NLC and MSE during 2003–2005 within intervals of 10 days. The NLC season lasts from the beginning of June to the end of July, while the MSE season starts a few days earlier and ends in mid-August. Therefore there is a shift of ~25 days between the beginning of summer as defined above and the start of the ice season. The ends of MSE and NLC seasons agree within approximately 1 week with the end of the summer season. Note that the NLC season ends earlier than the summer season while the MSE season lasts for some further days.

[32] As described above, ambient temperatures below the frost point and advection from polar latitudes are not sufficient for the existence of ice particles above Kühlungsborn. We speculate that the delayed start of the ice season is due to the fact that initial ice formation requires lower temperatures than ice existence. Our previously defined summer season (days 130–220) is based on the temperatures at 85 km altitude. For NLC existence, the shorter summer season at lower altitudes (for example, 83 km) has to be taken into account.

5.2. Comparison of NLC Occurrence With Mean Temperatures, Wave Amplitudes, and Meridional Wind

[33] The case studies above disclose additional requirements for NLC besides local supersaturation and advection from polar latitudes. In Figure 9, the nightly mean temperature profiles within June/July are plotted for nights with and without NLC. Only five out of the six nights from Table 2 are shown here because on the additional night (1/2 July 2004) the temperature coverage is too short (1 h) to be treated as a nightly mean. The nightly mean temperatures span the ranges 160–178 K and 145–165 K in 80 and 85 km, respectively. Interestingly, the lowest mean temperatures below 86 km are observed in a night without NLC. Because of the high temperature variability, the nightly mean temperatures are averaged for the whole June/July period and plotted with their standard deviation for nights with and without NLC. Between 80 and 90 km, the average temperature in NLC nights is up to 4 K lower than the average non-NLC temperature. However, this difference is within the standard deviations of the individual nights, and several non-NLC nights have been at least as cold as the NLC nights. The very low temperatures observed in a single NLC night above 85 km may be caused by the less than 3 h sounding time of this event, while the longer soundings with NLC are in the typical temperature range. We summarize that the average temperature of the NLC nights is slightly lower than of the non-NLC

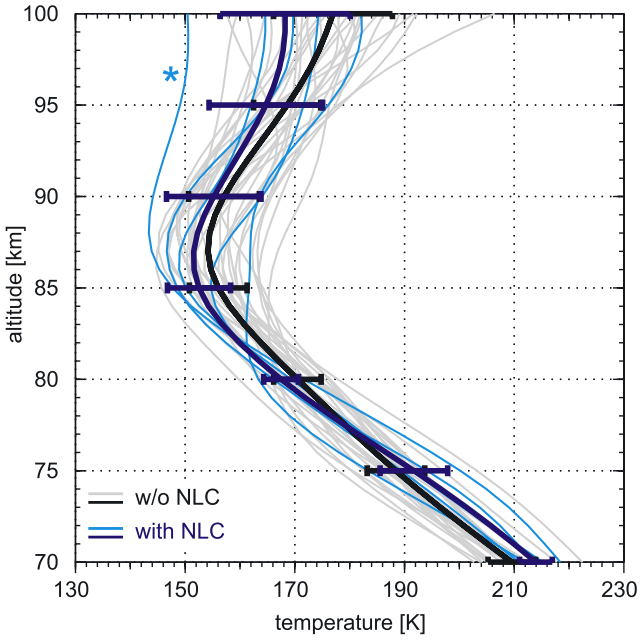

Figure 9. Nightly mean temperature profiles of June/July 2003–2005 (thin lines; light blue, 5 nights with NLC; grey, 28 nights without NLC). Only nights with more than 3 h sounding time are taken into account, except one additional NLC night (marked by asterisk). The thick lines give the summer mean profiles with their standard deviation, separated for nights with NLC (blue) and without (black).

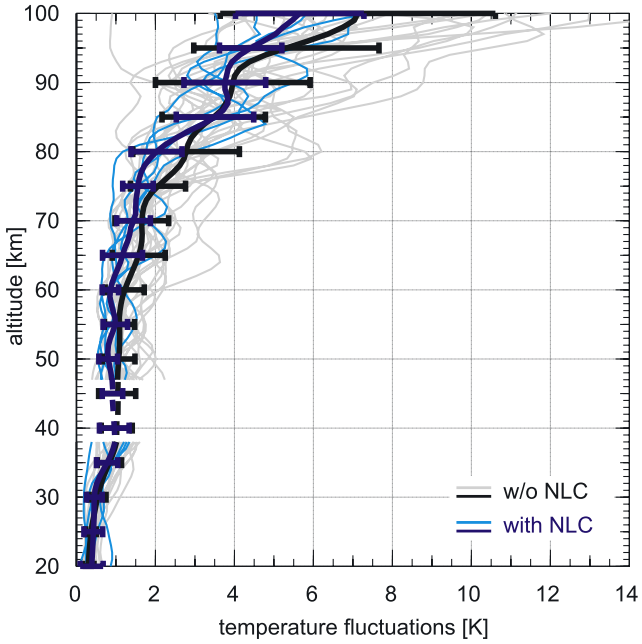

Figure 10. Nightly mean gravity wave activity of June/July 2003–2005 (thin lines; light blue, 5 nights with NLC; grey, 28 nights without NLC), cp. Figure 9. The thick lines give the summer mean profiles with their standard deviation, separated for nights with NLC (blue) and without (black).

cases, but very low temperatures are not sufficient for NLC observations.

[34] Also, the gravity wave activity derived from the local temperature profiles is not significantly different between nights with and without NLC. In Figure 10, nightly mean temperature fluctuations are presented. As described by *Rauthe et al.* [2006], these profiles represent the wave activity during the night between 20 and 100 km. Averages of the individual nightly mean profiles are calculated for the nights with and without NLC. Figure 10 reveals a slightly reduced wave activity of NLC nights above 50 km. However, the difference between NLC and non-NLC nights is much smaller than the variability within a single group of nights.

[35] Table 4 gives a summary of the number of supersaturated periods with and without NLC during the summers 2003–2005. Observations shorter than 2 h are neglected. In the table, all nights with supersaturation lasting longer than 1 h are summarized. Taking the lidar integration time of 30–60 min into account, this limit means that the supersaturation has to exist in at least two independent profiles. To account for the fact that NLCs occur most probably below 85 km, we have listed separate numbers for layers below and above 85 km. Supersaturated layers above 85 km may have produced ice particles, but these most likely small particles would not be visible as NLC, while MSE can not be observed during the night.

[36] Below 85 km, NLC exist in only ~20% of all nights with temperatures below the frost point. Even for high saturation ratios of $S > 10$, two thirds of all nights are lacking NLC within the same night above our station (though we have to admit a small statistic here). If we compare different altitudes, about two thirds of all supersaturated layers extend downward below 85 km (hence, allow NLC existence), while one third is limited to altitudes above 85 km. However, only about one fourth of the regions with $S > 10$ are observed below 85 km, while most of them are above this level. Therefore potentially higher saturation ratios can be found above 85 km altitude.

[37] To examine a possible correlation with the local wind field, the events in Table 4 are separated by the sign of the meridional wind (if available). Obviously, during all 10 events with supersaturation and simultaneous wind data below 85 km, a southward wind was prevailing for the whole supersaturated period or at least at the beginning. During 3 events out of these 10, the wind was changing to northward after a longer southward period. In summary, all NLC are observed during or after periods with southward-directed wind. We would like to note that also the prevailing wind is southward in summer at our location, with a dominating semidiurnal tide (not shown here). The mean meridional winds observed by the OSWIN radar in June/July 2005 at 85 km altitude reach the largest southward values near 9 UT (−20 m/s) and 21 UT (−35 m/s), while it is slightly northward near 4 UT (0–5 m/s) and 16 UT (0–5 m/s).

6. Discussion

6.1. General NLC Occurrence and Strength

[38] MSE and NLC are a rare phenomenon in midlatitudes (40°–60°N/S). *Wickwar et al.* [2002] report on a single NLC sounding by lidar at Logan (Utah, 41.7°N). This is, to the best of our knowledge, the southernmost observation of NLC. Other midlatitude NLC observations by lidar are, for example, reported from stations at 52.4°N [*Thomas et al.*, 1994], 54.1°N (our station) [*Alpers et al.*, 2000, 2001], and 54.6°N [*von Cossart et al.*, 1996]. Satellite soundings generally show decreasing NLC probability with decreasing latitude. In their review on satellite observations of polar mesospheric clouds (the satellite equivalent of NLC), *DeLand et al.* [2006] report an occurrence rate of PMC at 60°N of 3% and a southernmost latitude of 55°N for northern hemispheric PMC. Also, *Bailey et al.* [2005] treat the latitude-band of 50°–55°N as free of PMC and use this area for the estimation of the background radiation. Even if the different sensitivities of lidars and satellite instruments are taken into account, several former observa-

Table 4. Events With Supersaturation Between 10 May and 8 August for the Years 2003–2005[a]

	Overall	With NLC	Without NLC
Nights With S > 1	35	5	30
. . . thereof extension below 85 km	24	5	19
. . . . . thereof $v < 0$	7	4	3
. . . . . thereof $v > 0$	0	0	0
. . . . . thereof changing v (− → +)	3	0	3
Nights with S > 10	13	3	10
. . . thereof extension below 85 km	3	1	2
. . . . . thereof $v < 0$	2	1	1
. . . . . thereof $v > 0$	0	0	0
. . . . . thereof changing v (− → +)	1	0	1

[a]The number of nights with $S > 1$ ($S > 10$) for longer than 1 h is given. Particular emphasis is given to the region below 85 km because of the possible connection with NLC. These events are further separated by the ambient meridional wind. Note that wind data below 85 km are only available for part of the events with supersaturation.

tions confirm our location being right at the edge of the typical NLC (PMC) latitude range.

[39] NLC at Kühlungsborn are weak and dim compared to polar stations. The mean of the maximum volume backscatter coefficients β_{max} of the eight NLC observed since 2003 is $\overline{\beta_{max}} = \sim 1.3 \cdot 10^{-10}$ m^{-1}sr^{-1}. This is well below the number derived for example, at 69°N by the Arctic Lidar Observatory for Middle Atmosphere Research (ALOMAR) RMR lidar ($\overline{\beta_{max}} = 9.6 \cdot 10^{-10}$ m^{-1}sr^{-1}) [*Fiedler et al.*, 2003]. Of course, the detection limit for β_{max} is lower at Kühlungsborn because of the apparent nighttime conditions with less background and therefore less noise compared to higher latitudes suffering from polar day. If we artificially increase our detection limit to values well covered by the ALOMAR RMR lidar ($\beta > 4 \cdot 10^{-10}$ m^{-1}sr^{-1}), we still observe $\overline{\beta_{max}} < 6 \cdot 10^{-10}$ m^{-1}sr^{-1}. Therefore the different sensitivities explain only part of the difference in the observed NLC brightness. Taking only the strongest (brightest) NLC into account, we derive particle densities and particle radii which are comparable to the observations at polar latitudes [*von Cossart et al.*, 1999]. For dimmer NLC, the observation at three or more wavelengths is progressively awkward because of the different sensitivities of the lidars and laser wavelengths. By this, it is getting impossible to derive particle properties for most of the soundings, and it remains speculative whether for the many thin NLC above Kühlungsborn the ice particles are smaller or less in number.

6.2. Case Studies of NLC, Temperature, and Winds

[40] Most of the NLC and MSE were observed during the cold phase of the superposed gravity waves and at the lower edge of the supersaturated region. This has also been predicted by time-dependent two-dimensional models if the wave periods are longer than ~6 h [e.g., *Rapp et al.*, 2002]. However, in contrast to the model study (performed for polar conditions), in our observations the NLC often did not reappear after being destroyed during the warm phase (cp. Figure 3). The meridional wind component was always negative (southward) during the NLC events. This is of course a typical situation for midlatitude summer, while the reverse situation should be noted here again; for the few cases with northward wind during MSE, the radar echo often vanishes rapidly, i.e., within 1–2 h after the change of sign. In a more comprehensive study on all local MSE in the years 1998 and 2000–2005, a general increase in MSE during southward wind has been observed (Zeller, private communication, 2006).

[41] Model studies suggest that short-period gravity waves weaken NLC [*Klostermeyer*, 1998; *Rapp et al.*, 2002]. The NLC on 29/30 July 2004 appeared at moderate temperatures around the frost point and in the presence of comparatively strong short-period gravity waves (~1 h ground-based period). This is in some contrast to the model predictions and again clearly underscores the need for three-dimensional and time-dependent observations of wind, temperature, and humidity to allow the detailed examination of horizontal advection and local dynamics.

6.3. Supersaturation With and Without NLC

[42] There were several periods of $S > 1$ lasting longer than 1 h in the preceding summers (Table 4), sometimes reaching $S > 100$. However, only very few of them have persisted for the whole night (~4 h). While about 20% of the $S > 1$ events below 85 km are coupled with NLC, for the others the cold periods were too short, or the degree of saturation was still too low to form NLC particles within this particular air parcel. This is in general agreement with model calculations, where the process of NLC formation takes ~4–24 h depending on water vapor concentration and the size of condensation nuclei [*Rapp et al.*, 2002; *Berger and von Zahn*, 2002]. Therefore the existence of NLC (and mostly also of MSE) above our station is restricted to cases where the ice particles are advected from more polar locations. However, also supersaturated air-parcels without NLC have been advected from the north, so advection is a necessary but not sufficient condition. We examined whether there is a connection between gravity wave strength and NLC existence. However, from our data set, we have no indication that a low-gravity wave activity leads to the existence of NLC above our station. *Thayer et al.* [2003] and *Gerrard et al.* [2004] published a negative correlation of NLC backscatter coefficient and wave activity at 30 km altitude, i.e., NLC get stronger if the gravity wave activity in the stratosphere is low. Unfortunately, because of the small number of NLC above our site, we can not directly repeat this kind of analysis.

[43] Temperature profiles with and without colocated NLC were examined by *Petelina et al.* [2005] and *Wrotny and Russell* [2006] from satellite observations. They found the average temperature with NLC up to 10 K lower than the temperature without NLC. In the study of *Petelina et al.* [2005] the difference is larger than the standard deviation of the averaged profiles, but this study is limited to latitudes northward of 60°N. *Wrotny and Russell* [2006] average across the large latitude band of 55° to 70°N. There might be some aliasing effect because of the opposed mean meridional gradients of NLC probability and temperature. A standard deviation is not presented in this study.

[44] We summarize that the duration of supersaturated periods, the wind direction, the mean temperature, or gravity wave activity do not significantly differ with or without NLC. We suggest that the "history" of the advected air parcel is the most important parameter. The air parcels need to be continuously supersaturated for the last, for example, 10 h to allow the continuous existence of ice particles during the meridional transport. Only in the cold wave phases do the temperatures remain low enough to compete with the positive meridional temperature gradient.

6.4. Discussion of Water Vapor Pressure and Concentration

[45] For the calculation of the saturation ratio, the temperatures measured by the Institute of Atmospheric Physics (IAP) lidar have been combined with water vapor profiles taken from the LIMA model for the latitude of Kühlungsborn [*Sonnemann and Grygalashvyly*, 2005; Berger, submitted manuscript, 2007]. The water vapor concentration is ~3–5 ppmv below 85 km and decreases above. This is well within the range of available observations. Ground-based measurements of mesospheric water vapor by microwave sounders reveal mixing ratios of ~3 ppmv at 80 km in midlatitudes but provide no information above [*Nedoluha et al.*, 2000]. Unfortunately,

small-scale structures can not be resolved here because of long integration times of several days and averaging kernels of ~10–15 km. Other studies concentrate on the polar regions and suggest a water vapor concentration of more than ~6 ppmv in a layer around 83 km with dehydration above [*Summers et al.*, 2001; *McHugh et al.*, 2003]. Following the arguments of *Berger and Lübken* [2006], the above mentioned concentration might still be a lower limit for the true numbers. They describe water vapor enhancements by a factor of 10 at midlatitudes because of freeze-drying in higher latitudes. Of course, for the nights of supersaturation without NLC, we also can not totally exclude a local freeze-drying, even though a drying by ~90% is rather unlikely [*von Zahn and Berger*, 2003]. However, our main results are independent from the exact water vapor concentration, as the saturation ratio depends exponentially on temperature but only linearly on the water vapor mixing ratio.

[46] The water vapor pressure equation of *Marti and Mauersberger* [1993] has been applied to calculate the degree of saturation. Their formula is also suggested by *Rapp and Thomas* [2006], who presented an extensive discussion of the different published equations. We do not want to repeat this discussion but note that other equations would result in even higher degrees of saturation. Therefore the saturation ratios given in this study may even underestimate the true values.

7. Summary and Conclusions

[47] From 240 nights of lidar soundings during the years 2003–2005, a summer period between 10 May and 8 August (days 130 and 220, respectively) has been defined by the temperature at 85 km altitude. This period is further characterized by a mesopause being in the lower, summer state. Within summer, the average temperatures drop below the frost point temperature for about 15 days shortly after summer solstice. Despite that short period, MSE and NLC are irregularly observed above Kühlungsborn during an interval of ~70 and ~50 days, respectively. We have presented time-dependent temperature profiles showing the superposition of the mean temperatures by fluctuations of up to ±10 K at 85 km and ±20 K at 95 km due to gravity waves and tides. We find that temperatures occasionally fall below the frost point temperature for periods between some minutes and some hours, partly limited by our observation period in summer of ~4 h.

[48] MSE and NLC are sparse and dim above our site. Only eight NLC events and 250 h of MSE (with signal-noise ratio larger than 3 db) were observed in the summers of 2003–2005. All NLC soundings and some of the MSE observations are supplemented by simultaneous, colocated lidar temperature soundings. Ice existence is generally limited to periods with temperatures below the frost point, while sublimation can mostly be neglected. The observed NLC are always at the lower edge of the supersaturated region, with the maximum of supersaturation being 1–5 km higher than the NLC. The combined NLC/MSE and temperature soundings provide very good agreement with an estimated water vapor mixing ratio of 3–5 ppmv below 85 km, as given from a circulation model. On the other side, the observed temperature profiles reveal partly strong and/or long-lasting supersaturation without colocated NLC/MSE. For example, on 24/25 June 2005, temperatures below the frost point were observed during the whole sounding period (5 h), resulting occasionally in saturation ratios of $S > 100$. We conclude from our observations that temperatures much below the frost point and also horizontal advection from polar latitudes are not sufficient for the existence of ice particles above our site. While the NLC observations are coupled to the cold phases of waves and tides, the same air parcel has to be also cold enough for several hours prior to our sounding. If the ice particles sublimated once before they arrived above Kühlungsborn, generally the cold phases of gravity waves and tides are too short to generate fresh ice particles. In summary, NLC occurrence at Kühlungsborn is determined by advection and air-parcel history and less by local conditions of temperature and humidity. Therefore, for example, trend studies of NLC at midlatitudes have to account not only for changing temperature and humidity at a particular location but also for the ambient wind field.

[49] **Acknowledgments.** We would like to thank our colleagues at IAP and the numerous summer students for their help in the nighttime lidar soundings. T. Barth, T. Köpnick, M. Priester, and J. Trautner do valuable work in lidar/radar operation and maintenance. Water vapor data from the Leibniz-Institute Middle Atmosphere (LIMA) model was provided by Uwe Berger. Parts of this work were supported by the Deutsche Forschungsgemeinschaft (DFG) under the grants GE1625/1-1 and LU1174 (SOLEIL).

References

Alpers, M., M. Gerding, J. Höffner, and U. von Zahn (2000), NLC particle properties from a five-color lidar observation at 54°N, *J. Geophys. Res.*, *105*(D10), 12,235–12,240, doi:10.1029/2000JD900132.

Alpers, M., M. Gerding, J. Höffner, and J. Schneider (2001), Multiwavelength lidar observation of a strange noctilucent cloud at Kühlungsborn (54°N), *J. Geophys. Res.*, *106*(D8), 7945–7953, doi:10.1029/2000JD900666.

Alpers, M., R. Eixmann, C. Fricke-Begemann, M. Gerding, and J. Höffner (2004), Temperature lidar measurements from 1 to 105 km altitude using resonance, Rayleigh, and rotational Raman scattering, *Atmos. Chem. Phys.*, *4*(3), 793–800.

Avaste, O. A., A. V. Fedynsky, G. M. Grechko, V. I. Sevastyanov, and C. I. Willmann (1980), Advances in noctilucent cloud research in the space era, *Pure Appl. Geophys.*, *118*(1), 528–580, doi:10.1007/BF01586466.

Backhouse, T. W. (1885), The luminous cirrus clouds of June and July, *Meteorol. Mag.*, *20*, 133.

Bailey, S. M., A. W. Merkel, G. E. Thomas, and J. N. Carstens (2005), Observations of polar mesospheric clouds by the Student Nitric Oxide Explorer, *J. Geophys. Res.*, *110*, D13203, doi:10.1029/2004JD005422.

Berger, U., and F.-J. Lübken (2006), Weather in mesospheric ice layers, *Geophys. Res. Lett.*, *33*, L04806, doi:10.1029/2005GL024841.

Berger, U., and U. von Zahn (2002), Icy particles in the summer mesopause region: Three-dimensional modeling of their environment and two-dimensional modeling of their transport, *J. Geophys. Res.*, *107*(A11), 1366, doi:10.1029/2001JA000316.

DeLand, M. T., E. P. Shettle, G. E. Thomas, and J. J. Olivero (2006), A quarter-century of satellite polar mesospheric cloud observations, *J. Atmos. Sol.-Terr. Phys.*, *68*(1), 9–29, doi:10.1016/j.jastp.2005.08.003.

Ecklund, W. L., and B. B. Balsley (1981), Long-term observations of the Arctic mesosphere with MST radar at Poker Flat, Alaska, *J. Geophys. Res.*, *86*, 7775–7780.

Fiedler, J., G. von Cossart, and G. Baumgarten (2003), Noctilucent clouds above ALOMAR between 1997 and 2001: Occurrence and properties, *J. Geophys. Res.*, *108*(D8), 8453, doi:10.1029/2002JD002419.

Fricke-Begemann, C., M. Alpers, and J. Höffner (2002), Daylight rejection with a new receiver for potassium resonance temperature lidars, *Opt. Lett.*, *27*(21), 1932–1934.

Gerding, M., M. Alpers, U. von Zahn, R. J. Rollason, and J. M. C. Plane (2000), Atmospheric Ca and Ca^+ layers: Midlatitude observations and modeling, *J. Geophys. Res.*, *105*(A12), 27,131–27,146, doi:10.1029/2000JA900088.

Gerding, M., J. Höffner, and M. Rauthe (2007), Simultaneous observations of temperatures and ice-particles in the mid-latitude mesopause region, *Adv. Space Res.*, doi:10.1016/j.asr.2007.01.020, accepted.

Gerrard, A. J., T. J. Kane, J. P. Thayer, and S. D. Eckermann (2004), Concerning the upper stratospheric gravity wave and mesospheric cloud relationship over Sondrestrom, Greenland, *J. Atmos. Sol.-Terr. Phys.*, *66*(3-4), 229–240, doi:10.1016/j.jastp.2003.12.005.

Hedin, A. E. (1991), Extension of the MSIS thermosphere model into the middle and lower thermosphere, *J. Geophys. Res.*, *96*, 1159–1172.

Hocking, W. K., and T. Thayaparan (1997), Simultaneous and collocated observations of winds and tides by MF and meteor radars over London, Canada (43°N, 81°W), during 1994–1996, *Radio Sci.*, *32*(2), 833–865.

Jesse, O. (1885), Auffallende Abenderscheinungen am Himmel, *Meteorol. Z.*, *2*, 311–312.

Klostermeyer, J. (1998), A simple model of the ice particle size distribution in noctilucent clouds, *J. Geophys. Res.*, *103*(D22), 28,743–28,752.

Latteck, R., W. Singer, and J. Höffner (1999), Mesosphere summer echoes as observed by VHF radar at Kühlungsborn (54°N), *Geophys. Res. Lett.*, *26*(11), 1533–1536, doi:10.1029/1999GL900225.

Leslie, R. C. (1885), Sky glows, *Nature*, *32*, 245.

Lübken, F.-J., and J. Höffner (2004), Experimental evidence for ice particle interaction with metal atoms at the high latitude summer mesopause region, *Geophys. Res. Lett.*, *31*(8), L08103, doi:10.1029/2004GL019586.

Lübken, F.-J., K. H. Fricke, and M. Langer (1996), Noctilucent clouds and the thermal structure near the Arctic mesopause in summer, *J. Geophys. Res.*, *101*(D5), 9489–9508, doi:10.1029/96JD00444.

Lübken, F.-J., M. Zecha, J. Höffner, and J. Röttger (2004), Temperatures, polar mesosphere summer echoes, and noctilucent clouds over Spitsbergen (78°N), *J. Geophys. Res.*, *109*(D11), D11203, doi:10.1029/2003JD004247.

Marti, J., and K. Mauersberger (1993), A survey and new measurements of ice vapor pressure at temperatures between 170 and 250 K, *Geophys. Res. Lett.*, *20*, 363–366.

McHugh, M., M. Hervig, B. Magill, R. E. Thompson, E. Remsberg, J. Wrotny, and J. M. Russell III (2003), Improved mesospheric temperature, water vapor and polar mesospheric cloud extinctions from HALOE, *Geophys. Res. Lett.*, *30*(8), 1440, doi:10.1029/2002GL016859.

Morris, R. J., D. J. Murphy, A. R. Klekociuk, and D. A. Holdsworth (2007), First complete season of PMSE observations above Davis, Antarctica, and their relation to winds and temperatures, *Geophys. Res. Lett.*, *34*(5), L05805, doi:10.1029/2006GL028641.

Nedoluha, G. E., R. M. Bevilacqua, R. M. Gomez, B. C. Hicks, J. M. Russell III, and B. J. Connor (2000), Ground-based microwave observations of middle atmospheric water vapor in the 1990s, in *Atmospheric Science Across the Stratopause*, Geophys. Monogr., vol. 123, edited by D. E. Siskind, S. D. Eckermann, and M. E. Summers, pp. 257–270, AGU, Washington, D. C.

Petelina, S. V., D. A. Degenstein, E. J. Llewellyn, N. D. Lloyd, C. J. Mertens, M. G. Mlynczak, and J. M. Russell III (2005), Thermal conditions for PMC existence derived from Odin/OSIRIS and TIMED/SABER data, *Geophys. Res. Lett.*, *32*(17), L17813, doi:10.1029/2005GL023099.

Plane, J. M. C., B. J. Murray, X. Chu, and C. S. Gardner (2004), Removal of meteoric iron on polar mesospheric clouds, *Science*, *304*(5669), 426–428, doi:10.1126/science.1093236.

Rapp, M., and F.-J. Lübken (2004), Polar mesosphere summer echoes (PMSE): Review of observations and current understanding, *Atmos. Chem. Phys.*, *4*(11/12), 2601–2633.

Rapp, M., and G. E. Thomas (2006), Modeling the microphysics of mesospheric ice particles: Assessment of current capabilities and basic sensitivities, *J. Atmos. Sol.-Terr. Phys.*, *68*(7), 715–744, doi:10.1016/j.jastp.2005.10.015.

Rapp, M., F.-J. Lübken, A. Müllemann, G. E. Thomas, and E. Jensen (2002), Small-scale temperature variations in the vicinity of NLC: Experimental and model results, *J. Geophys. Res.*, *107*(D19), 4392, doi:10.1029/2001JD001241.

Rauthe, M., M. Gerding, J. Höffner, and F.-J. Lübken (2006), Lidar temperature measurements of gravity waves over Kühlungsborn (54°N) from 1 to 105 km: A winter-summer comparison, *J. Geophys. Res.*, *111*(D24), D24108, doi:10.1029/2006JD007354.

She, C. Y., and U. von Zahn (1998), Concept of a two-level mesopause: Support through new lidar observations, *J. Geophys. Res.*, *103*(D5), 5855–5863, doi:10.1029/97JD03450.

Singer, W., J. Bremer, W. K. Hocking, J. Weiss, R. Latteck, and M. Zecha (2003), Temperature and wind tides around the summer mesopause at middle and Arctic latitudes, *Adv. Space Res.*, *31*(9), 2055–2060.

Sonnemann, G. R., and M. Grygalashvyly (2005), Solar influence on mesospheric water vapor with impact on NLCs, *J. Atmos. Sol.-Terr. Phys.*, *67*(1-2), 177–190, doi:10.1016/j.jastp.2004.07.026.

Summers, M. E., R. R. Conway, C. R. Englert, D. E. Siskind, M. H. Stevens, J. M. Russell III, L. L. Gordley, and M. J. McHugh (2001), Discovery of a water vapor layer in the Arctic summer mesosphere: Implications for polar mesospheric clouds, *Geophys. Res. Lett.*, *28*(18), 3601–3604, doi:10.1029/2001GL013217.

Taylor, M. J., M. Gadsden, R. P. Lowe, M. S. Zalcik, and J. Brausch (2002), Mesospheric cloud observations at unusually low latitudes, *J. Atmos. Sol.-Terr. Phys.*, *64*, 991–999.

Thayer, J. P., M. Rapp, A. G. Gerrard, E. Gudmundsson, and T. J. Kane (2003), Gravity-wave influences on Arctic mesospheric clouds as determined by a Rayleigh lidar at Sondrestrom, Greenland, *J. Geophys. Res.*, *108*(D8), 8449, doi:10.1029/2002JD002363.

Thomas, G. E. (1991), Mesospheric clouds and the physics of the mesopause region, *Rev. Geophys.*, *29*, 553–575.

Thomas, G. E. (2003), Are noctilucent clouds harbingers of global change in the middle atmosphere?, *Adv. Space Res.*, *32*(9), 1737–1746, doi:10.1016/S0273-1177(03)90470-4.

Thomas, L., A. K. P. Marsh, D. P. Wareing, and M. A. Hassan (1994), Lidar observations of ice crystals associated with noctilucent clouds at middle latitudes, *Geophys. Res. Lett.*, *21*(5), 385–388.

von Cossart, G., P. Hoffmann, U. von Zahn, P. Keckhut, and A. Hauchecorne (1996), Mid-latitude noctilucent cloud observations by lidar, *Geophys. Res. Lett.*, *23*(21), 2919–2922.

von Cossart, G., J. Fiedler, and U. von Zahn (1999), Size distributions of NLC particles as determined from 3-color observations of NLC by ground-based lidar, *Geophys. Res. Lett.*, *26*, 1513–1516.

von Zahn, U., and U. Berger (2003), Persistent ice cloud in the midsummer upper mesosphere at high latitudes: Three-dimensional modeling and cloud interactions with ambient water vapor, *J. Geophys. Res.*, *108*(D8), 8451, doi:10.1029/2002JD002409.

von Zahn, U., and J. Höffner (1996), Mesopause temperature profiling by potassium lidar, *Geophys. Res. Lett.*, *23*(2), 141–144, doi:10.1029/95GL03688.

Wickwar, V. B., M. J. Taylor, J. P. Herron, and B. A. Martineau (2002), Visual and lidar observations of noctilucent clouds above Logan, Utah, at 41.7°N, *J. Geophys. Res.*, *107*(D7), 4054, doi:10.1029/2001JD001180.

Wrotny, J. E., and J. M. Russell III (2006), Interhemispheric differences in polar mesospheric clouds observed by the HALOE instrument, *J. Atmos. Sol.-Terr. Phys.*, *68*(12), 1352–1369, doi:10.1016/j.jastp.2006.05.014.

Zecha, M., J. Bremer, R. Latteck, W. Singer, and P. Hoffmann (2003), Properties of midlatitude mesosphere summer echoes after three seasons of VHF radar observations at 54°N, *J. Geophys. Res.*, *108*(D8), 8439, doi:10.1029/2002JD002442.

M. Gerding, J. Höffner, F.-J. Lübken, M. Rauthe, W. Singer, and M. Zecha, Leibniz-Institute of Atmospheric Physics, Schloss-Strasse 6, D-18225 Kühlungsborn, Germany. (gerding@iap-kborn.de)